For publication in IEEE Trans. Gee. Sci. and Remote Sens., 1994

Observations of Ocean Radar Backscatter at KU and C Bands in the Presence of Large Waves during the Surface Wave Dynamics Experiment

S. V. Nghiem, F. K. Li, S. H. Lou, and G. Neumann
Jet Propulsion Laboratory
California Institute of Technology
Pasadena, California, USA

R. E. McIntosh, S. C. Carson, and J. C. Carswell
Microwave Remote Sensing Laboratory
University of Massachusetts
Amherst, Massachusetts, USA

E. J. Walsh
NASA Goddard Space Flight Center
Wallops Flight Facility
Wallops Island, Virginia, USA

M. A. Donelan and W. M. Drennan
National Water Research Institute
Burlington, Ontario, Canada

Mailing address : Dr. S. V. Nghiem, Jet Propulsion Laboratory
Mail Stop 300-235, 4800 Oak Grove Drive, Pasadena, CA 91109

Observations of Radar Backscatter at Ku and C Bands in the Presence of Large Waves during the Surface Wave Dynamics Experiment

S. V. Nghiem, F. K. Li, S. H. Lou, and G. Neumann
Jet Propulsion Laboratory
California Institute of Technology
Pasadena, California, USA

R. E. McIntosh, S. C. Carson, and J. C. Carswell
Department of Electrical Engineering
University of Massachusetts
Amherst, Massachusetts, USA

E. J. Walsh[1]
NASA Goddard Space Flight Center
Wallops Flight Facility
Wallops Island, Virginia, USA

M. A. Donelan and W. M. Drennan
National Water Research Institute
Burlington, Ontario, Canada

Abstract — Ocean radar backscatter in the presence of large waves is investigated using data acquired with the Jet Propulsion Laboratory NUSCAT radar at K_u band for horizontal and vertical polarizations and the University of Massachusetts C-SCAT radar at C band for vertical polarization during the Surface Wave Dynamics Experiment. Backscatter

[1] Presently on assignment at NOAA Environmental Technology Laboratory, Boulder, CO

data of ocean surfaces was obtained in the presence of large waves with significant wave height up to 5.6 m. In moderate-wind cases, effects of large waves are not detectable within the measurement uncertainty and no noticeable correlation between backscatter coefficients and wave height is found. Under high wave light wind conditions, backscatter is enhanced significantly at large incidence angles with a weaker effect at small incidence angles. Backscatter coefficients in the wind speed range under consideration are compared with model results which confirm the experimental observations. Variations of the friction velocity, which can give rise to the observed backscatter behaviors in the presence of large waves, are presented.

I. INTRODUCTION

Radar scatterometry is a technique for remote sensing of the near surface wind speed and direction over the ocean. Sensors have been successfully developed and flown at Kuband on the SEASAT [1] satellite in 1978, and at C band on the operational ERS-1 satellite [2]. The small scale ocean surface roughness increases with increasing local winds, and this increased roughness enhances the off-nadir radar cross section of the ocean. This indirect relationship forms the basis of using radar scatterometry for ocean wind measurements. The relationship can be modified when waves with large significant wave heights (SWH), caused by strong winds earlier or by swells propagating into the local area, are present. In this case, the accuracy of radar scatterometry in retrieving the ocean surface wind field can be affected by the presence of such large waves.

The effects of high waves on ocean radar backscatter have been investigated with theoretical models. Based upon a model for a wind-driven sea with swells, Durden and Vesecky [3] predict that a very large amplitude swell can significantly increase the backscatter coefficients at low radar frequency (L band), small incidence angle and light wind; however, they predict that the effects will be small at K_u band and large incidence angles for all wind

speeds, Donelan and Pierson [4] indicate that a swell traveling at a large angle oblique to the wind direction can have an important impact on scatterometry. This is the case especially for light wind and low incidence angles because the backscatter extrema are not necessarily in the local wind direction, At larger incidence angles, this model suggests that the large-wave effects diminish because the contribution of specular backscatter becomes less important as compared to the Bragg contribution for the short wave part of the composite spectrum. Plant [5,6] applies the principle of the conservation of wave action to modeling the interactions between long and short waves on the water surface by using a hydrodynamic modulation transfer function, This model indicates that the long-wave properties can also affect the normalized radar cross section of the ocean through the second-order effects of short-wave tilting and hydrodynamic modulation. In the calculation of backscatter coefficients in this model, however, the long and short waves are assumed to be local wind generated, and therefore the direction of these waves are aligned.

Experimentally, tower based measurements at L- and KU-band frequencies [7] have been made to study the radar dependence upon ocean waves. Horizontally polarized backscatter data at L band were taken at incidence angles of 35° and 45°, and azimuthal angles from 225° through North to 60°. Vertically polarized K.-band data were collected only at 45° incidence angle, with azimuthal angles limited to 300° to 360°. Most of the long waves encountered during this experiment were not generated by the local wind. At lower wind speeds, these measurements suggest that radar cross sections may be slightly lowered when long waves propagate at a large angle to the wind. At the C band frequency of 5.3 GHz, airborne measurements [8] were obtained for radar cross section as a function of wind speed. The data seem to indicate that the upwind/crosswind ratio is the largest when the wind blows in the wave direction, The implications of these experiments are tentative and need further data for their confirmation.

This paper presents a case study of radar backscatter from the ocean surface at K_u and C bands in the presence of large waves. The data was acquired during the Surface Wave

Dynamics Experiment (SWADE) in 1991 when two airborne scatterometers were flown together on the NASA Ames C130B aircraft: NUSCAT, a K.-band scatterometer developed at the Jet Propulsion Laboratory (JPL), and C-SCAT a C-band scatterometer developed at the University of Massachusetts (UMass). The plane flew over an instrumented oceanic area off the U.S. East coast near 37° North latitude and 74° West longitude. Backscatter coefficients obtained on 4 March, 1991 in the presence of swells with SWH as high as 5.6 m are compared with data at lower SWH under similar wind conditions. Wind speeds were in both moderate and light wind ranges, Although the observations were limited to a narrow set of conditions, they represent a quantitative evaluation of the variation in the radar cross sect ion in the presence of large waves at two different radar frequencies. In addition, several buoys measured atmospheric and oceanic parameters, another airborne radar acquired directional wave spectra, and a ship was deployed to make measurements including friction velocities. The backscatter measurements are also compared with calculations from empirical and theoretical models.

Section 11 below shows the data sets selected for this study and the results for observations of radar backscatter in the presence of large waves and section 111 compares the experimental measurements with model results. The appendix describes in details the NUSCAT and C-SCAT scatterometers, the SWADE location, the experimental scenario, the directional wave fields, and sea surface temperature effects.

II. RADAR OBSERVATIONS IN THE PRESENCE OF LARGE WAVES

A, Data Selection

A specific scatterometer data set was chosen from the SWADE data base in which the SWH was high and was compared with data sets taken at lower SWH to evaluate the effects of large waves. The criteria for the data selection were: (1) the measurements had the same polarization and incidence angle, (2) the wind speeds for these cases were

close ($\lesssim 1$ m $\cdot s^{-1}$ difference), (3) the backseat ter data were collected at the location nearest to the buoy in question, and (4) Gulf Stream boundary crossings with potential complications in the ocean conditions were avoided. These criteria were chosen to isolate cases with high and low SWH while the other scatterometer and oceanic parameters were as similar as possible, As table Al and figures A4 and A5 in the appendix show, large significant wave heights occurred predominantly during flight 5 on 4 March, 1991. Data sets collected under high SWH conditions were selected first, and then corresponding cases with low SWH were chosen using the criteria listed above. Table A 1 indicates that the ocean conditions measured by the buoys at different locations can be quite different. This suggests that the winds were very inhomogeneous spatially. This was especially true of the data collected at buoy A, where several cases of light to very low winds were observed. Since this buoy was in the cold, shallow, near shore waters where the ocean conditions were quite different from the other buoys, none of this data was used. In general, the low SWH cases used for comparison came from flight 9 for moderate wind speed cases, and flight 6 for low wind speed cases.

The wind speeds for the high and low SWH cases were, in general, not exactly the same, and since the normalized radar cross section of the ocean is strongly dependent upon the wind, a scheme was developed to account for the wind difference. Consider a case with low SWH where the wind speed is close but not the same as the wind in a case with high S WH. Denote the measured backseat ter coefficients by $\sigma^{\ell M}_{HH}$ for horizontal polarization and $\sigma^{\ell M}_{VV}$ for vertical polarization. The subscript, $PP = HH$ or VV, is the transmit ted and received polarization. The superscript, ℓ, represents low S WH conditions, Define $U^{\ell B}_N(19.5)$ to be the neutral wind speed at 19.5 m derived from the co-located buoy wind measurement. The subscript, N, stands for neutral wind speed which is derived from the buoy measurement using the formulation by Large and Pond [9]. Similarly, $U^{hB}_N(19.5)$ represents buoy derived neutral wind speed during high SWH. Since, the wind measurements from the buoys are available only on an hourly basis, we linearly interpolated

the data to provide a continuous set for comparison, The selected radar measurements were within 25 minutes of the actual buoy wind measurements.

The backseat ter coefficients, $\sigma_{PP}^{\ell B}$ and σ_{PP}^{hB}, are calculated by applying the derived neutral wind speeds to the SASS-II model function [10,11]. The difference $\Delta\sigma_{PP}$

$$\Delta\sigma_{PP} = \sigma_{PP}^{hB} - \sigma_{PP}^{\ell B} \tag{1}$$

is added to the measured backscatter coefficient $\sigma_{PP}^{\ell M}$, to adjust this measurement to the wind conditions corresponding to the high SWH case. The new value is referred to as the adjusted backscatter coefficient and is expressed as

$$\sigma_{PP}^{\ell R} = \sigma_{PP}^{\ell M} + \mathrm{Au}_{pp} \tag{2}$$

These adjusted cross section measurements were then used to study the effects of swells on the radar backscatter. This normalization method involves incremental differences in the wind speeds and the normalized radar cross section estimates. Thus, the adjusted backscatt er coefficient, $\sigma_{PP}^{\ell R}$, is not very sensitive to cross-calibrations between SASS and NUSCAT. In addition, if the compared data sets include only in-situ wind measurements from the same buoy, the results will depend only on relative rather than absolute calibrations of the buoy instruments.

B. Large Waves and Moderate Winds

This section investigates the effects of long waves with large SWH on the radar backscatter during moderate wind conditions. In this case, the SASS-II geophysical model function predictions agree with the adjusted results. Figure la and lb show the comparison of NUSCAT radar backscatter measurements near Discus E at 40° incidence angle for vertical and horizontal polarization, respectively. These and the subsequent results are shown as a function of azimuthal angle (relative to upwind; plotted continuously without the 360° wrapping around; this continuous increase in azimuth corresponds to the increase

in data acquisition time). In figure 1a, the normalized radar cross section measurements were collected on 4 March, 1991 and 8 March, 1991. During these measurements, the SWH was 5.5 m on 4 March, 1991 and 1.7 m on 8 March, 1991. The neutral wind speed was $U_N^{hB}(19.5)$ = 12.0 m · s-ion 4 March, 1991 and $U_N^{\ell B}(19.5)$ = 12.4 m · s-ion 8 March, 1991, Using (1) and (2), this 0.4 $m \cdot s^{-1}$ wind speed difference reduces $\sigma_{VV}^{\ell M}$ by an average of 0.23 dB. In figure lb, a case for the horizontal polarization is shown. For this case, the SWH was 5.4 m on 4 March, 1991 and 1.9 m on 8 March, 1991. The neutral wind speed was $U_N^{hB}(19.5)$ = 11.8 $m \cdot s^{-1}$ on 4 March, 1991 and $U_N^{\ell B}(19.5)$ = 11.2 $m \cdot s^{-1}$ on 8 March, 1991, The adjustment for the wind speed difference increases $\sigma_{VV}^{\ell M}$ by an average of 0,48 dB. Figure 1 shows no obvious distinction in the radar backscatter for vertical or horizontal polarization between the low and high SWH data sets.

In addition to these data sets, we also compared low and high SWH data sets at other incidence angles. We have adopted the following approach to present the results in a concise manner. Wind estimates were obtained from the observed NUSCAT results by fitting the SASS-II model function to the data. These estimates are referred to as the apparent neutral wind speed, $U_N^{\ell A}$ (19.5) and U_N^{hA} (19.5). The superscripts ℓ and h signify low or high SWH conditions, respectively,

Again, to account for the slight differences in actual wind speeds between the low and high SWH data sets, $U_N^{\ell A}(19.5)$ is adjusted for the difference. The adjustment is obtained by the difference in the buoy wind measurements:

$$\Delta U_N^B = U_N^{hB} - U_N^{\ell B} \tag{3}$$

where the argument (19.5) has been dropped to simplify the expression. These differences were used to adjust the apparent wind, obtained by fitting NUSCAT measurements to SASS-II, for the low SWH data to the wind conditions of the high SWH data. The result will be referred to as the recovered apparent wind $U_N^{\ell A}$ for low SWH conditions and is given as

$$U_N^{\ell R} = U_N^{\ell A} + \Delta U_N^B \tag{4}$$

The two apparent winds, $U_N^{\ell R}$ and U_N^{hA}, are then compared to evaluate quantitatively the influence of large waves on radar backscat ter during moderate winds,

Table 1 gives results of this comparison, The cases are for vertical polarization at incidence angles 30° and 40° and horizontal polarization at incidence angles 20°, 30°, 40°, and 60°. For each case, at least two measurements at low SWH are compared to the corresponding measurement at high S WH. Included in the table are the measurements of S WH, air temperature, and sea temperature. The air temperature was less than the sea temperature in all cases. This indicates the Monin-Obukov stability lengths (L) are negative and thus the atmospheric boundary layer conditions are unstable. The small differences, $\delta U = U_N^{\ell R} - U_N^{hA}$, and the percent error, $\%E = 100(\delta U / U_N^{hA})$, presented in table 1 demonstrates no significant effects of swells on the backscatter measurements collected by NUSCAT at K.-band for moderate wind conditions. Furthermore, the apparent wind speeds derived from the NUSCAT measurements agree well with the in-situ wind measurements. Figure 2 compares the apparent wind speed and direction to the buoy measurements of wind speed and direction. The cases shown are for high SWH conditions.

The C-SCAT data were analyzed using similar techniques. The backscatter coefficients σ_{vv} were compared for low and high SWH conditions under moderate winds. Figure 3 shows a representative example for 40° incidence angle, This data corresponds to the NUSCAT data shown in figure la. Both sets were collected during the same flight line. The neutral winds speed for these sets are $U_N^{\ell B}(19.5) = 12.4$ m , s^{-1} and $U_N^{hB}(19.5) = 12.0$ $m \cdot s^{-1}$. The adjustment in $\sigma_{VV}^{\ell M}$ to account for the wind difference is less than 0.3 dB. The comparison in figure 3 reveals no visible difference between the magnitude nor the azimuthal modulation of the backscatter measurements.

We compared additional C-SCAT data sets at 20°, 30°, 40°, and 50° incidence angle. At each angle, there were several high and correspondingly low SWH cases. The neutral wind speeds at 10 m ranged from 9.1 $m \cdot s^{-1}$ to 11.8 $m \cdot s^{-1}$. Figures 4a and 4b summarize the results. Figure 4a is a plot of the upwind/crosswind ratio versus SWH. There is no

observable effect on the upwind/crosswind ratio caused by the large waves. Figure 4b displays the average backseat ter coefficient versus SWH. The average was performed over the entire 360° for each case. No adjustment is made for the differences in wind speeds. This plot demonstrates no significant change in the magnitude of the average backscatter coefficient at C-band with SWH for moderate winds.

C. Large Waves and Light Winds

During SWADE, a couple of flights occurred during light wind conditions. The SWH varied from 1.7 m to 3,4 m for these data sets. Applying the same criteria defined in section II.A to these data, we investigated the effects of large waves on the radar backscatter for light winds. The two flights of interest were on 4 March, 1991 and 5 March, 1991. The data was collected near Discus C. Figure A4a shows the wind and SWH conditions at Discus C during the flight on 4 March, 1991. Table Al summarizes the these conditions for both flights.

The comparison data, selected after the criteria in II.A, were backscatter measurements at horizontal polarization for incidence angles from 20° to 50° for NUSCAT and at vertical polarization for incidence angles in the same range for C-SCAT. Tables 2 and 3 summarize the data for NUSCAT and C-SCAT, respectively. They list the wind speed (measured by buoy at 4-m height), SWH, air temperature T_{air}, and sea temperature T_{sea} obtained from Discus C for each low and high SWH set. The differences in wind speeds between the low and high SWH sets range from 0,1 m . s^{-1} to 1.3 m . s^{-1}.

Figures 5a and 5b compare data collected at 40° incidence angle for low and high SWH. Figure 5a is a plot of σ_{HH} collected by NUSCAT and figure 5b is a plot of σ_{VV} collected by C-SCAT. The data is displayed over the full azimuth range and is referenced to the *upwind* direction, defined (for this subsection) as the direction of maximum backscatter. The actual angles will be dealt with later in figure 8. The K.-band measurements are approximately 5 dB higher for the high wave case compared to the low wave, Likewise, the

C-band measurements are approximately 4.5 dB higher for the high wave case. For these measurements, the air temperature is approximately the same while the sea temperatures are quit e different.

Backscatter for high wave conditions is represented by closed circles in figure 6. This data was also collected at 30° incidence angle and horizontal polarization with a sea temperature of 14.9° C. The high S WH measurements show an enhanced radar cross section in comparison 'to the two low SWH cases. At incidence angles from 20° to 50°, figures 7a and 7b compare the conditions corresponding to the cases listed in table 2 for NUSCAT and table 3 for C-SCAT, respectively. This comparison shows an increase of several dB in the backscatter coefficient between the high and low SWH cases . The difference seems to increase with incidence angle.

Figures 8a and 8b compare the time evolution of the wind vectors deduced from NUSCAT data to the wind vectors obtained from the buoys. The black circles in figure 8a represent the "apparent" wind speed (at 19.5 m) which was obtained by a least-square-error fit of the SASS-II model function to the NUSCAT data collected over Discus C. The open circles are the '<average" wind speed derived by translating the buoy wind measurements to 19.5 m using the Large and Pond formulation [9], The average wind speeds shown at 54, 114, and 174 minutes after 21:00 UT were 8 minute averages recorded by the buoys at 22:00, 23:00, and 24:00 UT. Each average was performed during minutes 50 to 58 before the recorded hour. The other data points shown were interpolated from these measurements and integrated over the corresponding duration of the NUSCAT measurement. Figure 8b shows the principal directions of the peak wave components obtained from the NDBC directional wave spectrum measurements. The wave direction is defined as the angle from North to the direction to which the wave propagates, The wave data from the buoy are measured from minute 28 to 48 each hour, The average is plotted at minute 38 before the hour. The other wave data points correspond to time-interpolated buoy data over the scatterometer time.

As figure 8a and figure A4a show, the wind speed at Discus C dropped quickly at the beginning of the flight to a light wind speed, and then began to increase during the flight. Coast al Buoy 2 shows similar conditions. The apparent winds in figure 8a are higher than the average winds, implying that the observed backscatter is higher than the model function estimates for the given buoy wind. Both the apparent wind and the average wind follow the same trend, They drop in the beginning of the flight and then increase slightly towards the end. In the latter part of the flight, the apparent wind becomes closer to the average wind, The direction of the apparent wind, shown in figure 8b, appears to be different from both the average wind direction and the principle wave direction. Towards the end of the flight, the apparent wind direction appears to be closer to the average wind direction. For the times shown, the peak wave direction was between 340° to 360° and the SWH was between 3 and 4 m .

For light winds, the data presented in this section indicate that ocean radar backscatter is larger in cases of high waves especially at larger incidence angles. These observations were seen in both KU-band and C-band backscatter while similar ocean conditions were measured by two nearby buoys Discus C and Coastal Buoy 2 (see figure A4).

III. COMPARISONS WITH MODELS

The experimental measurements obtained by NUSCAT and C-SCAT are compared with calculated results from empirical models such as SASS-II [10,11] for K_u band, CMOD3-H1 for C band [12], and a theoretical model [5,6] for both frequencies. Figure 9a shows the comparisons between the models and NUSCAT data at vertical polarization and 40° incidence angle. NUSCAT data plotted with open squares in Figure 9a are the same as those for the large wave case in figure la (SWH=5.5m on 4 March, 1991). SASS-II results represented by the thick curve are calculated from the model function, The wind was calculated to be 12.0 m · s^{-1} at a height of 19.5 m using the buoy data. The thin curve is

the calculated results from Plant's model for wind-generated waves using a 10-m wind of 11.3 m. s^{-1} derived from the 19.5 m wind used in SASS-II. While the models do not include swells, all results match well. This again indicates that the effect of the large waves at moderate winds is not significant in our case study,

Similarly, the models are compared with the C-band data corresponding to the above Ku-band data. The results are shown in figure 9b. Both the CMOD3-H1 and Plant's model use the wind U(10) = 11.3 m $\cdot s^{-1}$ derived from the buoy data, The models agree well with the data except at the crosswind direction where Plant's model underestimates the backscatter.

In the case of high SWH and light winds, the data presented in panels c and d of figure 9 correspond to the high SWH cases shown in figure 5. The incidence angle in this figure is 40°. In the model calculations, $U(19.5)$ = 6.6 m $\cdot s^{-1}$ and $U(10)$ = 6.3 m . s^{-1} are used in the SASS-H and Plant's models for KU band, respectively. Results at C band are calculated from the CMOD3-H1 and Plant's models using U(10) = 5.4 m . s-1. The K_u- and C-band measurements are as much as 4 dB higher than SASS-II and CMOD3-H1 models. Plant's model for both frequencies gives backseat t er which is even lower than the other two models,

A mechanism for large wave effects on backscatter is the superposition of a large-scale roughness caused by swells on the wind-generated roughness. Durden and Vesecky [3] estimated that a large magnitude swell of 16 m in SWH or 4 m in root-mean-square height with a 300-m wavelength could cause 4.5 to 3 dB increase in K.-band horizontal backscatter at 20° and only 1,5 to 1 dB at 50° for wind speeds at 5 to 10 $m \cdot s^{-1}$. In the same wind speed range, an increase of 6-4,5 dB at 20° and 3-1,5 dB at 50° incidence angle was obtained for L-band backscatter. This model predicts that the effects of swells decreases as the incidence angle increases because at small incidence angles, the backscatter is partly due to specular return; while at large incidence angles, specular return is negligible, This wave superposition mechanism predicts a trend with incidence angle different from that

observed in the data.

Another potential mechanism that contributes to the backscatter is wave breaking. Phillips and Banner [13] showed that long waves moving across the surface can augment the surface drift near the long-wave crests; consequently, the maximum amplitude of the short waves before breaking is reduced and the number of waves breaking is increased. In the results shown in [14], the backscatter due to wave breaking was suggested to be directly related to the cubic magnitude of the friction velocity and therefore increases as the friction velocity increases. The backscatter measurements in this paper, however, show the opposite trend,

Ocean radar backscatter has been suggested to be closely related to the friction velocity, u_* [15]. Let's consider the variations in u_* in the presence of swells measured during SWADE. The Small Water Pkme Area - Twin Hull, SWATH, ship Frederick G. Creed was chartered and equipped to perform measurements, including u_*, in support of SWADE [16]. For the above large-wave cases, the flight lines did not pass over the temporal or spatial vicinity of the SWATH ship; therefore, co-located measurements of u_* were not available to correlate with the scatterometer observations. Instead, u_* measurements in the presence of large swells are evaluated for a qualitative comparison. Tables 4 and 5 show the times, locations, atmospheric and oceanic parameters for these cases.

In these swell cases, data from the SWATH ship show measured values of u_* corresponding to the larger values found in the last column of table 4. For instance, in SWATH ship Run 25 started at 23:09 on 5 March, 1991, the friction velocity was 0.26 m · s-land the neutral wind speed was 3,72 m $\cdot s^{-1}$. At this neutral wind speed and the measured air and sea temperatures, Large and Pond's formula [9] gives u_* = 0,14 m $\cdot s^{-1}$ without consideration of swell effects. The difference between the value of u_* without swell and the measured value with swell is 0.12 m · S-l. With the exception of Run 24, all other cases in table 5 show differences in the order of 0.1 m $\cdot s^{-1}$ bet ween u_* measurements in the presence of swells compared to u_* calculations without swell. Similar increments in u_* *are*

observed in moderate wind conditions (8.6 m . s^{-1} to 9.7 m . s^{-1} at 12.9 m) in the presence of large wave of equivalent SWH, These results are summarized in table 5.

The above observations lead to the hypothesis that the increase of *u.* in the presence of swells is responsible for the effects in the observed backseat ter. Figure 10 presents the backscatter calculated with a model function relating the mean normalized radar cross section to *u.* [17]. This model was developed based on the backseat ter measured by the JPL K.-band Airborne Microwave Scatterometer and the measured *u.* during the Frontal Air-Sea Interaction Experiment. The results in figure 10 show that an increase of 0.1 m , s-* in u_* (as suggested by the SWATH ship measurements in the swell cases) can give rise to a 3.5-dB increase in σ_{HH} at 30° and a 4.5-dB increase at 50° incidence angle at light wind conditions. For the same magnitude of increment in u_* at moderate winds, the change in the backscatter is less significant (σ_{HH} varies only by 1.5 dB) compared to the case of light winds as seen in figure 10. These results follow the observations of the backscatter in the presence of swells.

Another trend in the observed backscatter for the swell cases is that the increase in the backseat ter is less at small incidence angles (see figure 7). At the small angles, ocean backseat ter coefficients measured by scatterometers [8,18-20] become less sensitive to wind variations. Moreover, in the power-law model function relating mean backscatter to u_* [17], the exponent of *u.* for 30° incidence angle is about 20% less than that for 50°, Hence, the increase in u_* will result in a weaker increase in the backscatter at small angles of incidence. This corresponds to the small enhancement at small incidence angles observed in σ_{VV} and σ_{HH}, shown in figure 7 for the KU- and C-band frequencies. Thus, the increase of the friction velocity in the swell cases also gives the same trend of smaller increase in backseat ter at small incident angles as seen in the measurements.

In summary, the backscatter measurements at K_u and C bands obtained during SWADE were used to study the behavior of the backscatter in the presence of large waves. The experimental observations are : (1) For moderate wind conditions, there was no obvi-

ous difference between the backseat ter measurements observed for low and high S WH; (2) For light winds, however, the backscatter coefficients were significantly enhanced in the presence of large swells; and (3) The enhancement also seemed to increase with incidence angle, especially for the KU-band data. These observations are different from the trends predicted by wave superposition [3] and wave breaking [13-14] mechanisms. However, an increase of the friction velocity in the presence of swells can lead to results which agree with the experimental observations.

APPENDIX

Al. NUSCAT and C-SCAT Scatterometers

During SWADE, NUSCAT and C-SCAT, the two airborne scatterometers, collected backscatter data. NUSCAT is a KU-band system operating near 14 GHz. The system comprises of an antenna subsystem, an RF subsystem, a data collection subsystem, and a controller as illustrated in figure Ala, The antenna is a parabolic dish with a peak gain of 32 dB and an equivalent beamwidth of 4°. The antenna was placed inside a radome on the tail of the C-130B aircraft (see figure A2), and was mounted on a gimbal, which was used to rotate it in complete azimuthal scans at selected elevation (incidence) angles. The antenna subsystem is connected through a rotary joint to the RF subsystem, from which horizontally (H) or vertically (V) polarized pulses are transmitted with a peak power of either 10 or 250 W at a repetition frequency of 4 to 10 kHz and a pulse length of 15 to 75 us. When the system transmits either H or V polarization, two receivers collect simultaneous co- and cross-polarized returns. The radar echoes from each pulse are amplified, down-converted to I/Q samples and digitally square-law detected. The returns from multiple echoes are integrated over a 0,5 second interval, and then recorded on computer compatible tapes,

C-SCAT is a pulsed, low-power scatterometer operating with vertical polarization in

the frequency band of 4,98-5.70 GHz with a peak power of 2 W. The radar system consists of a spinning antenna, a transmitter/receiver subsystem, digital interface electronics, and a computer control and data acquisition subsystem shown in figure A 1 b. The antenna is a flat microstrip array with a peak gain of 28 dB, and an antenna equivalent beamwidth of about 5°, A spinning mechanism rotates the whole antenna in a full azimuthal circle at around 20 rpm. The incidence angle can be steered from 20° to 50° by frequency scanning. The transmitted pulse duration is adjusted with aircraft altitude as an input to maximize the signal-to-noise ratios of the received echoes. Further details of C-SCAT have been reported in [21].

The internal system calibration for NUSCAT is performed by injecting the transmit signal into the receiver through a calibration loop. The relative calibration accuracy involves the uncertainty in the measurements of transmitted power, receiver gain, the orientation angles of the antenna, the aircraft altitude, the rotary joint loss, the radome loss and the attenuators. The relative calibration accuracy is estimated to be ± 0.23 dB. The measured radar backscatter accuracy depends on the number of independent samples and the signal-to-noise ratio (SNR). The operating frequency was dithered over 100 MHz to generate additional independent samples (N) which effectively reduce the statistical fluctuation of the detected power by $1/\sqrt{N}$. For the observations reported in this paper, N is between 750 and 5000. It should be noted that the SNR and the accuracy of the noise-only measurements was high enough that the backscatter power accuracy was primarily determined by the number of independent samples. The absolute accuracy of NUSCAT was subjected to other error sources such as attenuator loss, calibration loop loss, antenna gain, beamwidth, and various losses from the waveguide and the rotary joint, The antenna gain was determined by the three-horn measurement method at the JPL antenna range. The system stability and absolute accuracy were evaluated by taking data over the ocean surface at 10° incidence angle, where the backscatter is insensitive to surface roughness conditions [19]. These in-flight calibrations were performed at the beginning and the end

of each flight line during SWADE. Based on these measurements, our estimated absolute error is about ±1 dB.

C-SCAT is subject to the same sources of error as NUSCAT, and requires similar calibration measurements. The internal system is calibrated by feeding part of the transmit signal into the receiver through a series of attenuators to calibrate out system fluctuations, which are typically less than 0.1 dB during a flight. Additionally, the C-SCAT system was absolutely calibrated using a trihedral corner reflector at the UMass campus and a sphere at Goldstone, California. The relative precision is better than 0.25 dB, and the absolute accuracy is estimated to be within 1 dB [21],

During SWADE, the NUSCAT antenna was stepped in azimuth for 10° once every 4 seconds. NUSCAT collected azimuthal scans of data at various incidence angles, ranging from 0° to 60° in 10° increments. The C-SCAT antenna was rotated at 20 rpm, and the backscatter data were averaged into 5° azimuthal bins. Each rotation collects approximately 30 independent samples in each bin, and the data from at least 2 azimuthal scans were averaged together to obtain a stable average of the normalized radar cross section. C-SCAT collected azimuthal scans of data at incidence angles ranging from 20° to 50° in 10° increments.

In both the NUSCAT and C-SCAT data, the aircraft speed, altitude, latitude, longitude, yaw, pitch and roll angles were recorded. The actual values of the incidence and azimuthal angles were calculated from the commanded pointing angles and the aircraft pitch and roll angles. The variations in the aircraft pitch and roll induced fluctuations in the incidence angles at which the radar data was taken, For the NUSCAT data, the SASS-II model function [10,11] was chosen to adjust the backscatter values due to the fluctuations in incidence angle, These variations were subtracted from the measured data to obtain values corresponding to the commanded incidence angle. This technique has been shown to be relatively insensitive to the model function chosen for the range of wind speed and incidence angle variations [22]. A similar procedure was applied to the C-SCAT

data base, with the fitting function derived from the C-SCAT data base with a harmonic functional form.

AZ. S WADE Experimental Scenario

The Surface Wave Dynamics Experiment (SWADE) occurred in October 1990 to March 1991. Among its purposes was to study the effects of large waves on ocean backscatter. The experimental area, located off the coast of Maryland and Virginia (as depicted in the map in figure A3), was an instrumented ocean area. As the map shows, several buoys are anchored in the area: Discus C (C), Discus E (E), Discus N (N), CERC, and the National Oceanographic and Atmospheric Administration's Experimental buoy, or Costal Buoy 2 (A). During the experiment, NUSCAT and C-SCAT were flown on the C-130B aircraft to take radar backscatter data over ocean surfaces. There were a total of 10 frights during the period 2 February, 1991 to 9 March, 1991. The flights were partitioned into flight lines, and each line into runs. Flight patterns among the buoys included straight, triangle and radiator patterns. The oceanic conditions encompassed wind speeds ranging from 2 to 12 $m \cdot s^{-1}$ and significant wave heights ranging from below 1 m to above 5 m. Table 1 summarizes the flight patterns for the 10 flights, together with the oceanic parameters measured by the buoys.

During flight 5 on 4 March, 1991, backscatter data were acquired between 20:10 and 00:15 (UT) the following day. Although the wind was from the West, the wave field was dominated by a large swell from the South. The buoy measurements from the National Data Buoy Center (NDBC) provide a synoptic view of the sea conditions. In figure A4, the wind speed at 4 m above the ocean surface (top panel), wind direction (middle panel), and significant wave height (bottom panel) obtained by 3 buoys are plotted as functions of time, with the flight time indicated by bold horizontal bars over the time scale. The wind data were averaged for a duration of 8 minutes from 10 to 2 minutes before the tag hour; e.g., the wind data obtained between 22:50 and 22:58 were averaged and reported as the

average wind speed at 23:00. The wave data is averaged from 28 to 48 minutes before the hour, and similarly recorded.

The plots in figure A4a at Discus E on 4 March, 1991 reveal a very strong wind, up to 16.7 m · s-l, from 237°. This strong wind occurred approximately 3 hours before the flight and dropped to a moderate westerly wind of 10 m . s^{-1} during the flight. Similarly, the wind speed at Discus C subsided from moderate to a light wind, as low as 4.2 m. s^{-1}, and then picked up again at the end of the flight (see the black circle curve in figure A4a). The wind direction observations at Discus N, Discus E, and at CERC from 21:00 on March 4 through 00:00 on March 5 ranged from 235° to 277°. At Discus C, only the last two observations were outside this range (327° and 116°). The dominant long-wave wavelength at Discus E was 244 m throughout this four hour flight, and its direction of propagation was within 5° of 357°, At Discus N, the dominant wavelength fluctuated between 244 m and 192 m, and the direction of propagation was within 5° of 349°. The SWH varied spatially, being the highest (5.6 m) at the discus buoy furthest offshore (E), and the lowest (3.4 m) at the discus buoy furthest to the West (CERC) at 21:00. The wave height slowly decreased over the experiment during the four hour period (at 00:00, 5 March, 1991, the SWH was 5,1 m at Discus E and 2.9 m at CERC).

The range of wind speeds corresponding to the swell cases is similar to the wind range encountered in several other flights where the wave heights were lower (see table Al), For example, the SWH at buoy E on March 8 in flight 9 was 2.5 m or less while the wind speed at 4 m above the ocean surface was in the moderate range of 10-12 m.s-^{1}, which overlaps the wind speed range in the case with the large SWH (Discus E, March 4, flight 5). For light winds, table Al indicates that the wind speeds cover an overlapping range at Discus C during flight 5, and during flight 6 at CERC, while the SWH measured at the buoys are different by a factor of 2. This data set presents an opportunity to study the effect of large waves on ocean backscatter by comparing backscatter coefficients at K_u and C bands for cases with low and high waves under similar wind conditions. Furthermore, data from

the Scanning Radar Altimeter are available for the swell characterization with directional wave fields shown in the next section.

A3. Directional *Wave Fields*

Figure A5 shows four directional wave spectra obtained by the Scanning Radar Altimeter (SRA) on westerly ground tracks. The spectrum in the top panel (A) was acquired at 21:04:26 from 625 m altitude near Discus E and the results are compared with the 21:00 Discus E observations. The along track and cross track spacings of the SRA data to generate the directional wave spectra were 12.2 m and 7.8 m, respectively, making it impossible to observe wavelengths shorter than about 25 m propagating in an easterly direction and about 16 m propagating in a northerly direction. The direction of propagation is in good agreement with the buoy observations, Both the SRA directional wave spectrum and the Discus E nondirectional wave spectrum indicate a wave system concentrated in the longer wavelengths,

The SRA spectrum in the second panel (B) of figure A5 was acquired at the same position as the one in panel A, but two hours later, and it is compared with the Discus E data at 23:00. This SRA spectrum and the two below it were generated from data acquired from an altitude of 1250 m, with the footprint and cross track elevation point spacing double what they were for the top panel, Despite the change in measurement geometry and the passage of time, the two spectra are essentially the same. The third panel (C) was acquired at 23:02:39 midway between Discus E and Discus C. We used it to compared to the Discus C observations at 23:00.

The wave field is significantly reduced at the Discus C position relative to Discus E, but the same trend in propagation direction with increasing frequency is persistent. The spectrum in the bottom panel (D) was acquired at 23:17:25, just inshore of the Costal Buoy 2, It is compared with the 00:00 Discus C observations from 5 March, 1991. Panels C and D indicate that the wave field at Discus C changed little temporally over that hour interval,

but the direction of propagation at the spectral peak measured by SRA changed spatially, shifting about 40° toward the West as the SRA moved closer to shore. This is probably an influence of the shallower water close to shore. Panels A and B of figure A5 indicate that the wind direction in the vicinity of Discus E was approximately at right angles to the direction of propagation at the peak of the directional wave spectrum at Discus E. Panel D indicates that the wind was nearly opposite to the dominant wave direction near Costal Buoy 2. Figure A4 indicates that the wind at Coastal Buoy 2 and Discus C abruptly shifted about 70° northward at 22:00 and 23:00, respectively. This was the same interval when the wind speed was decreasing rapidly, and these recent light winds had not had time to influence even the higher frequencies (0.32 Hz) of the buoy spectra shown by the dashed lines in panels C and D of figure 5A. These directional wave spectra together with the buoy data provide the basis for the study on backscatter in the presence of swells.

A4. Sea Surface ***Temperature***

In the comparison of backscatter for the cases of large wave and light wind conditions (section H. C), there are differences in the sea surface temperature. Hence, the effects of the sea temperature need to be investigated to isolate the effects of the swells.

The difference in sea surface temperature can cause a difference in the viscosity. In turn, the viscosity can effect the roughness of the sea for a given wind speed. Donelan and Pierson [4] indicate that the backscatter increases as the temperature of the sea increases and that this effect can be significant for light winds when the temperature difference is large (O° C to 30° C). However, for the temperature range 14° C to 36° C, wave tank measurements [23] at X band (vertical polarization) showed no observable difference in the backscatter at winds $U(19.5)$ from 5 to 25 m · s-l.

To evaluate the effects of sea temperature on our data, two cases will be considered where all parameters are essentially the same except for the sea temperature. If sea surface temperature plays a dominant role, the backscatter should be higher in the case where the

temperature is higher. On 5 March, 1991 and 6 March, 1991 the sea temperature was 18.8°C and 9.0°C, respectively. Table 2 gives a summary of the conditions and figure 6 compares the data, showing backscatter measurements at 30° incidence angle, horizontal polarization during low wave conditions. Open circles represent the data collected for T_{sea} = 18.8° C on 5 March, 1991 and pluses represent data collected for T_{sea} = 9.0°C on 6 March, 1991. The two low wave backseat ter measurements are approximately the same, even though the sea temperature is different by more than a factor of two. Since all other conditions were basically the same, we conclude that the effects of sea temperature are negligible for these data sets.

Additionally, the air temperature is nearly constant, varying from T_{air} = 9.3° C on 5 March, 1991 to T_{air} = 11.1°C on 6 March, 1991. The atmosphere under these air and sea conditions is slightly unstable, and this instability increases with increasing sea temperature. Previous observations have shown an increase in the backscatter coefficient of the ocean surface with increasing atmospheric instability [24]. However, the atmospheric stability for these cases is small (z/L varies from —0.2 to —0.5), and the expected change in radar cross section is negligible, Donelan and Pierson [4] also predict a difference of less than 1 dB per 10"C at these wind speeds (5 m · s-l). Thus, the temperature difference would not cause a large backscatter difference in these cases,

ACKNOWLEDGMENT

The research described in this paper was carried out by the Jet Propulsion Laboratory, California Institute of Technology, under a contract with the National Aeronautics and Space Administration. Donelan and Drennan acknowledge the support of the Office of Naval Research under grant number NOOO14-88-J-1O28. The authors thank Dr. J. D. Oberholtzer and Dr. K. Steele for the buoy data, Dr. I. Popstefanija for additional C-SCAT data, and Dr. W. Plant for the ocean backscatter model.

REFERENCES

[1] W. L. Jones, L. C. Schroeder, D. H. Boggs, E. M. Bracalente, R. A. Brown, G. J. Dome, W. J, Pierson, and F. J. Wentz, "The SEA SAT-A Satellite Scatterometer: the Geophysical Evaluation of Remotely Sensed Wind Vector over the Ocean," *J. Geophys. Res.*, vol. 87, no. C5, pp. 3297-3317, 1982.

[2] E, P. W. Attema, "The Active Microwave Instrument On-board the ERS-1 Satellite," Proceedings *of the IEEE*, vol. 79, no, 6, 850-866, 1991.

[3] S. L. Durden and J. F. Vesecky, "A Physical Radar Cross-section Model for a Wind-driven Sea with Swell," *IEEE J. Ocean, Engineer.*, vol. OE-10, no. 4, pp. 445-45], 1985.

[4] M. A. Donelan and W. J. Pierson, "Radar Scattering and Equilibrium Ranges in Wind-generated Waves with Application to Scatterometry," *J. Geophys. Res.*, vol. 92, no. C5, pp. 4971-5029, 1987.

[5] W. J, Plant, "A Two-scale Model of Short Wind-generated Waves and Scat terometry," *J. Geophys. Res.*, vol. 91, no. C9, pp. 10735-10749, 1986.

[6] W. J. Plant, Correction to "A Two-scale Model of Short Wind-generated Waves and Scat terometry," *J. Geophys. Res.*, vol. 93, no. C2, pp. 1347, 1988.

[7] W. C. Keller and W. J. Plant, "Cross Sections and Modulation Transfer Functions at L and Ku Bands Measured During the Tower Ocean Wave And Radar Dependence Experiment ," *J. Geophys. Res.*, *vol.* 95, no. C9, pp. 16277-16289, 1990.

[8] F. Feindt, V. Wismann, W, Alpers, and W. C. Keller, "Airborne Measurements of the Ocean Radar Cross Section at 5.3 GHz as a Function of Wind Speed," Radio *Sci.*, vol. 21, no. 5, pp. 845-856, 1986.

[9] W. G. Large and S, Pond, "Open Ocean Momentum Flux Measurements in Moderate to Strong Wind," *J. Phys. Oceanogr.*, vol. 11, 324-336, 1981.

[10] F. J. Wentz, S. Peteherych, and L. A. Thomas, "A Model Function for Ocean Radar Cross Sections at 14.6 GHz," *J. Geophys. Res.*, vol. 89, no. C3, pp. 3689-3704, 1984,

[11] F. J. Wentz, L. A. Mattox, and S. Peteherych, "New Algorithms for Microwave Measurements of Ocean Winds: Applications to SEA SAT and the Special Sensor Microwave Imager," *J. Geophys. Res.*, vol. 91, no. *C2,* pp. 2289-2307, 1986.

[12] A, E. Long, "C-band V-polarized Radar Sea Echo Model from ERS-1 Haltenbalken Campaign," *URSI* Microwave *Signature Conf.*, IGLS-Innsbruck, Austria, July 1-3, 1992.

[13] O. M. Phillips and M, L. Banner, "Wave Breaking in the Presence of Wind Drift and Swell," *J. Fluid Mech.*, vol. 66, no. 4, pp. 625-640, 1974.

[14] O. M. Phillips, "Radar Returns from the Sea Surface - Bragg Scattering and Breaking Waves," *J. Phys. Oceanogr.*, vol. 18, 1065-1074, 1988,

[15] F. Li, W. Large, W Shaw, E. J. Walsh, and K. Davidson, "Ocean Radar Backscatter Relationship with Near-Surface Winds: A Case Study during FASINEX," *J. Phys. Oceanogr.*, vol. 19, no. 3, pp. 342-353, 1989.

[16] K. B, Katsaros, M. A. Donelan, and W. M, Drennan, "Flux Measurements from a SWATH Ship in SWADE," *J. Marine Systems,* no, *4,* pp. 117-132, 1993.

[17] D. E. Weissman, K. L. Davidson, R. A. Brown, C. A. Friehe, and F. Li, "The Relationships Between the Microwave Radar Cross Section and both Wind Speed and Stress – Model Function Development Using FASINEX Data," accepted for publication in *J, Geophys. Res.*, 1993.

[18] L. C. Schroeder, D. H. Boggs, G. Dome, I. M, Halberstam, W. L. Jones, W. J. Pierson, and F. J, Went z, "The Relationship between Wind Vector and Normalized Radar Cross Section Used to Derive SEASAT-A Satellite Scatterometer Winds," *J. Geophys. Res.*, vol. *87,* no. *C5,* pp. 3318-3336, 1982,

[19] W. L. Jones, L, C. Schroeder, and J. L, Mitchell, "Aircraft Measurements of Microwave Scattering Signature of the Ocean," *IEEE Trans. Antennas Propagat.*, *vol. AP-25,* no. 1, pp. 52-61, 1977.

[20] H. Masuko, K. Okamoto, M, Shimada, and S, Niwa, "Measurement of Microwave

Backscattering Signatures of the Ocean Surfaces Using X and K_a Band Airborne Scatteromet ers," *J. Geophys. Res.*, vol. 91, no, Cll, pp. 13065-13083, 1986.

[21] D. J. McLaughlin, R. E. McIntosh, A. Pazmany, L. Hevizi, and E. Boltniew, "A C-band Scatterometer for Remote Sensing the Air-sea Interface," *IEEE Trans. Geosci. Remote Sens.*, vol. *29,* no. *2,* pp. 260-267, 1991.

[22] F. K. Li, G. Neumann, S. Shaffer, and S. L. Durden, "Studies of the Location of Azimuth Modulation for K_u Band Ocean Radar Backscatter," *J. Geophys. Res.*, vol. *93,* no. *C7,* pp. 8229-8238, 1988.

[23] M. R. Keller, W. C. Keller, and W. J. Plant, "A Wave Tank Study of the Dependence of X Band Cross Sections on Wind Speed and Water Temperature," *J. Geophys. Res.*, vol. 97, no. C4, pp. 5771-5792, 1992.

[24] W. C. Keller, W. J. Plant, and D. J. Weissman, "The Dependence of X-Band Microwave Sea Return on Atmospheric Stability and Sea State", *J. Geophys. Res.*, vol. *90,* no. Cl, pp. 1019-1029, 1985.

LIST OF FIGURES

and 30° incidence angle between high-wave case represented by black circles and low-wave cases denoted with open circles and plus signs at different sea surface temperatures,

Figure 7 Comparisons of backscatter coefficients versus incidence angles in the upwind and crosswind directions between high-wave cases represented by black symbols and low-wave cases denoted with open symbols: (a) NUSCAT horizontal polarization and (b) C-SCAT vertical polarization.

Figure 8 Time evolution of (a) Wind speeds and (b) Wind directions. Directions of dominant waves are also shown,

Figure 9 Comparisons of measured backseat ter coefficients (squares) in the presence of swells at 40° incidence angle to results calculated from empirical models (thick curves) and Plant's t heretical model (thin curves), For moderate wind (a) NUSCAT vertical polarization for U(10) = 11.3 $m \cdot s^{-1}$ and (b) C-SCAT vertical polarization for U(10) = 11.3 m . s-l. For light wind (c) NUSCAT horizontal polarization for U(10) = 6.6 m . s^{-1} and (d) C-SCAT vertical polarization for U(10) = 5.4 m . s^{-1}.

Figure 10 Backscatter coefficient σ_{HH} at K_u band versus friction velocity at 30° and 50° incidence angle. The results are obtained from the model function relating mean backscatter to friction velocity [17].

Figure Al Scatterometer system block diagrams: (a) NUSCAT and (b) C-SCAT.

Figure A2 Locations of NUSCAT and C-SCAT antennas on the NASA Ames Research Center C- 130B aircraft,

Figure A3 Geographical location where the Surface Wave Dynamics Experiment was carried out. Encircled capital letters denote buoy positions: A is the NOAA Coastal Buoy 2, C is Discus C, E is Discus E, N is Discus N, and R is CERC.

Figure A4 Data for (a) Wind speeds at height of 4 m and (b) Significant wave heights measured by Discus E and Discus C about one day (4 March, 1991) before Flight 5 for scatterometer measurements until one day (5 March, 1991) after the flight. The flight duration is indicated with the bold horizontal bar.

Figure A5 Directional wave spectra measured by the NASA Scanning Radar Altimeter compared with the direction of propagation and spectral variance density measured by SWADE pitch-and-roll buoys. The contour lines on the right side of the figure indicate SRA measurements of absolute spectral density in 1.5 dB increments above a floor of 0.02 m^2 Hz^{-1} per degree. The dashed curves on the right side indicate the direction of propagation measured by the buoy. The continuous vertical lines indicate the direction from which the wind was blowing and the dashed vertical lines represent the direction toward which the wind was blowing (to be consistent with the wave propagation directions), The top panel (A) compares a SRA wave spectrum measured at 21:04:26 in the vicinity of N 37.5°, W 73.5° with the Discus E 21:00 observations. The second panel (B) compares a 22:58:13 SRA spectrum at the same location with the 23:00 Discus E observations. The third panel (C) compares a 23:02:39 SRA spectrum acquired near N 37.51°, W 73.85° with the 23:00 Discus C observations, and the bottom panel (D) compares a 23:17:25 SRA spectrum near N 37.73°, W 74.84° with the 00:00 Discus C observations on 5 March, 1991.

LIST OF TABLES

Table 1 Comparisons between high-wave (bold faced) and low-wave cases: Pol and θ_0 are antenna polarization and incidence angle in degrees. The apparent wind speed U_N^A is U_N^{hA} for high-wave cases (bold faced) or $U_N^{\ell A}$ for low-wave cases. Similarly, the buoy wind speed U_N^B is U_N^{hB} or $U_N^{\ell B}$ for high (bold faced) and low waves, respectively. $U_N^{\ell R}$ is the recovered wind speed. All wind speeds are in m . s^{-1} at 19.5 m. $\delta U = U_N^{\ell R} - U_N^{hA}$ *and* $\%E = 100(\delta U/U_N^{hA})$ are the difference in $m \cdot s^{-1}$ and the percent age error. H_s is significant wave height in m. T_{air} and T_{sea} *are* air and sea temperatures in $°C$.

Table 2 Buoy data corresponding to high (bold face) and low-wave cases for comparisons NUSCAT backscatter coefficients. Wind speeds is U(4) measured at 4m height, significant wave height is H_s, air temperature is Z'$_{ai}r$, and sea surface temperature is T_{sea}.

Table 3 Buoy data corresponding to high (bold face) and low-wave cases for comparisons C-SCAT backseat ter coefficients. Wind speed U(4) is measured at 4-m height, significant wave height is H_s, air temperature is T_{air}, and sea surface temperature is T_{sea}.

Table 4 Results for u_*, measured by the SWATH ship, under light winds in the presence of large waves. T_{air} is air temperature, T_{sea} is sea surface temperature, H_s is significant wave height, ϕ_{wave} is for direction to which waves propagate, $U(12.9)$ is wind speed measured at 12.9-m height, ϕ_{wind} is wind direction, Exp. u_* *is* from the experiment in the presence of swells, and Cal, u_* is calculated [14] without swell.

Table 5 Results for *u.,* measured by the SWATH ship, under moderate winds in the presence of large waves. T_{air} is air temperature, T_{sea} is sea surface temperature, H_s is significant wave height, ϕ_{wave} is for direction to which wave propagates, $U(12.9)$ is wind speed measured at 12,9-m height, ϕ_{wind} is wind direction, Exp. u^* *is* from the experiment in the presence of swells, and Cal. u_* is calculated [14] without swell.

Table Al Flight patterns and ocean conditions during SWADE. The unit for flight time is UT, wind vector $\vec{U}$ is $\mathrm{m \cdot s^{-1}}$ for speed and degree for direction (measured at 4-m height), and significant wave heights H_s is m. Events represented by bold-faced characters are used for the comparison of high and low waves at moderate wind speeds; events represented by italic characters are for the comparison at light winds.

(a) NUSCAT W at 40-degree Incidence

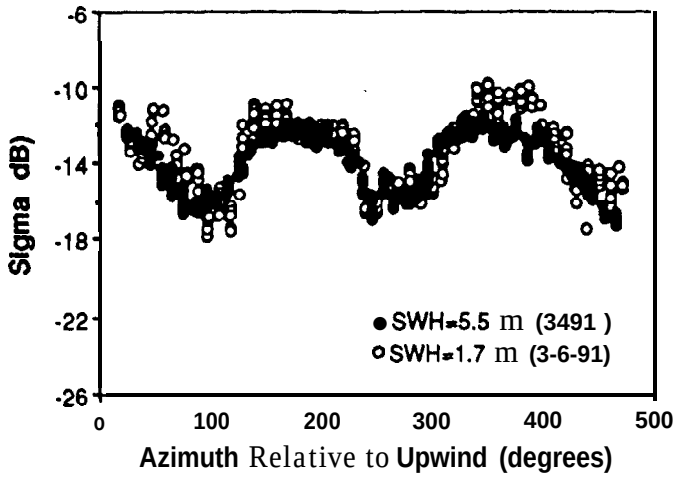

(b) NUSCAT HH at 40-degree Incidence

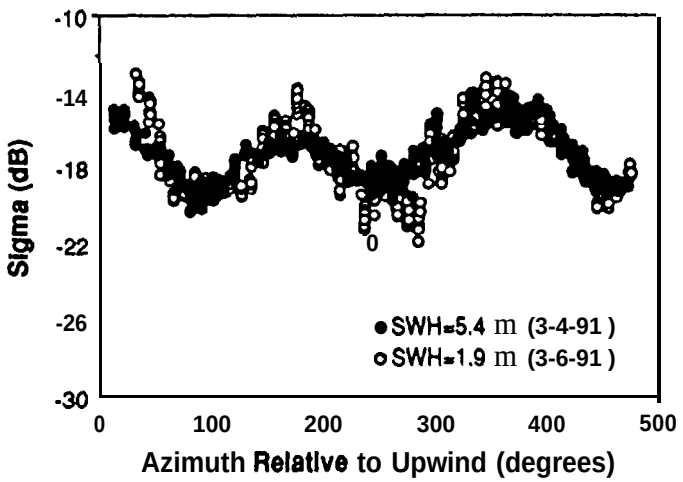

FIG 1

(a) Comparison of Wind Speeds

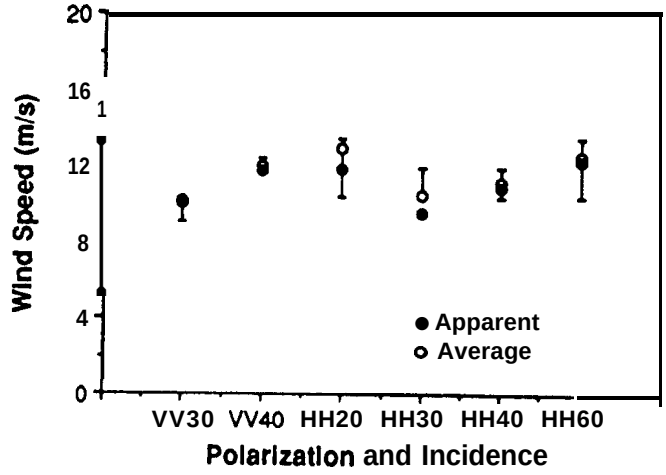

(b) Comparison of Wind Directions

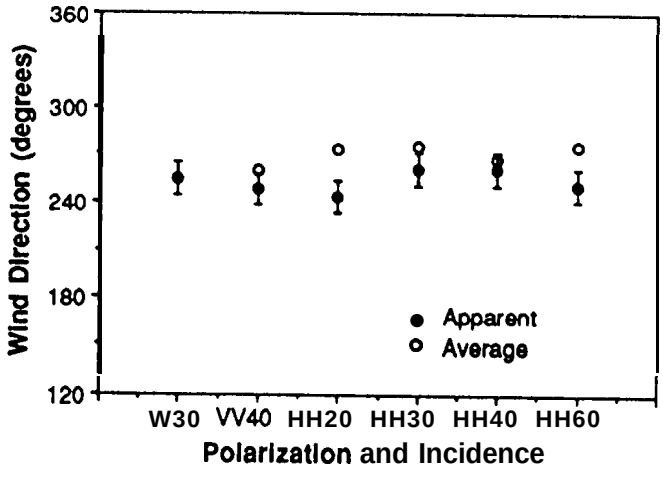

FIG 2

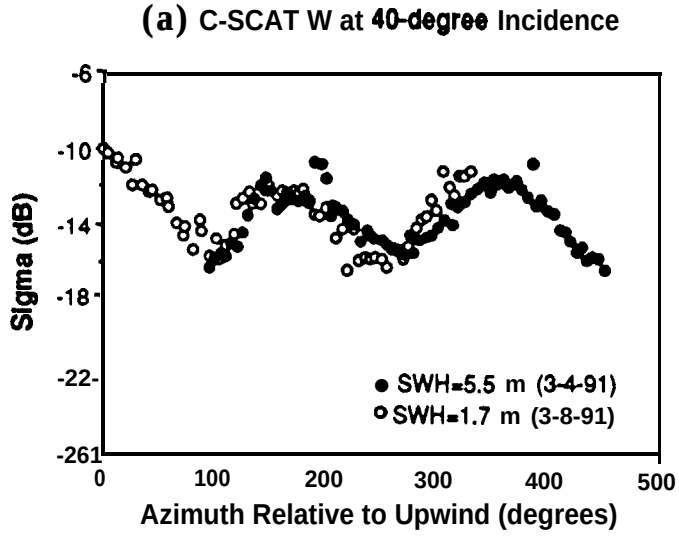
(a) C-SCAT W at 40-degree Incidence
Sigma (dB)
-6
-10
-14
-18
-22
-26
0
100
200
300
400
500
Azimuth Relative to Upwind (degrees)
● SWH=5.5 m (3-4-91)
o SWH=1.7 m (3-8-91)

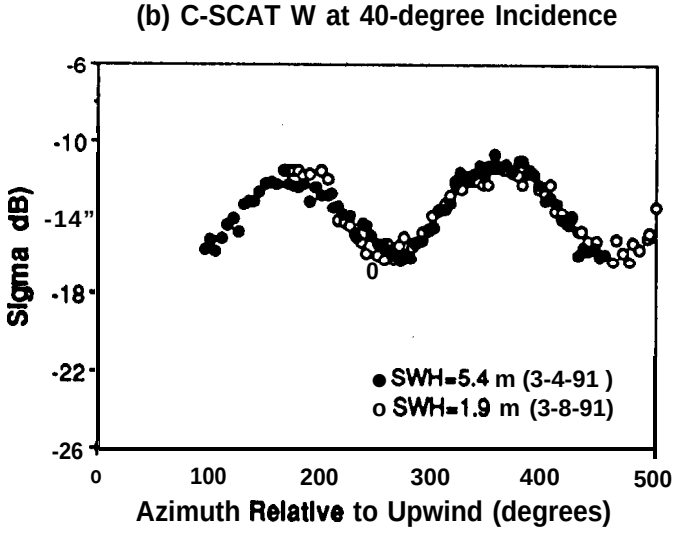
(b) C-SCAT W at 40-degree Incidence
Sigma dB)
-6
-10
-14
-18
-22
-26
0
100
200
300
400
500
Azimuth Relative to Upwind (degrees)
● SWH=5.4 m (3-4-91)
o SWH=1.9 m (3-8-91)

FIG 3

(a) C-SCAT W Up/Cross Wind Ratio

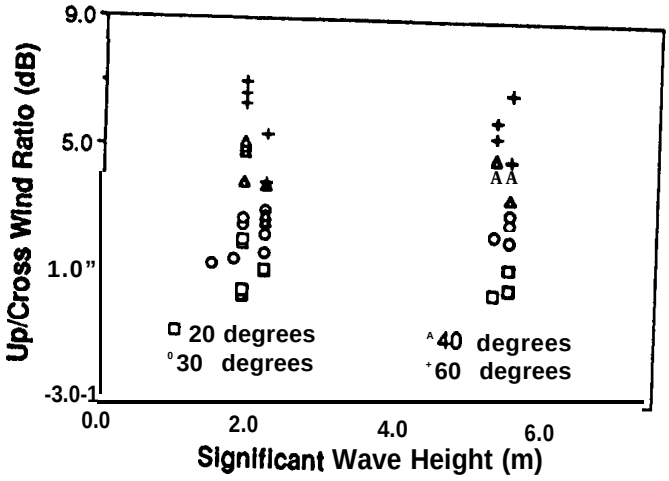

(b) C-SCAT W Average Sigma

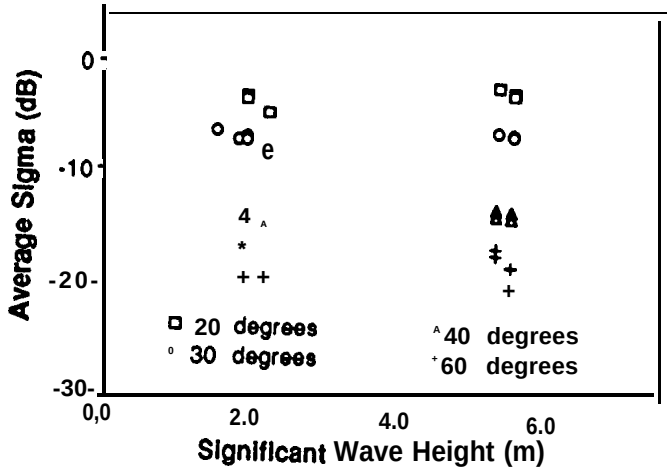

FIG 4

(a) NUSCAT HH at 40-degree Incidence

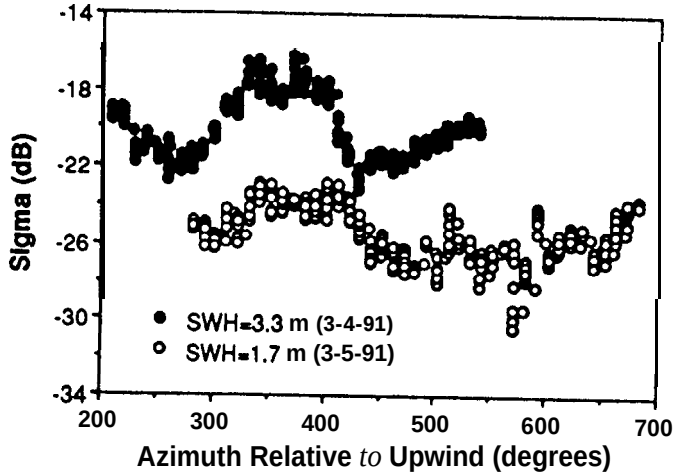

(b) C-SCAT W at 40-degree Incidence

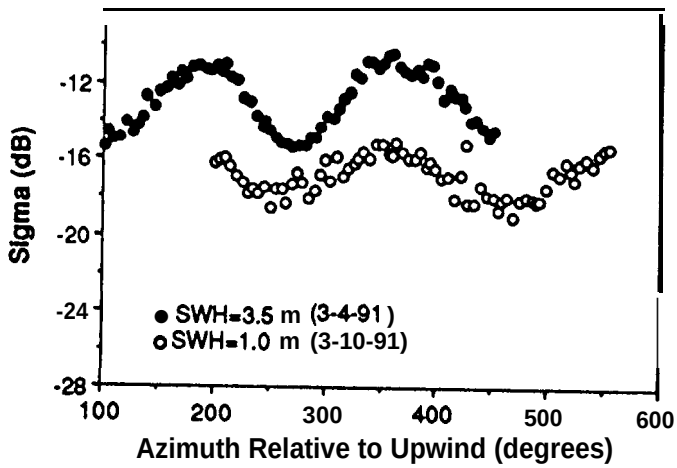

FIG 5

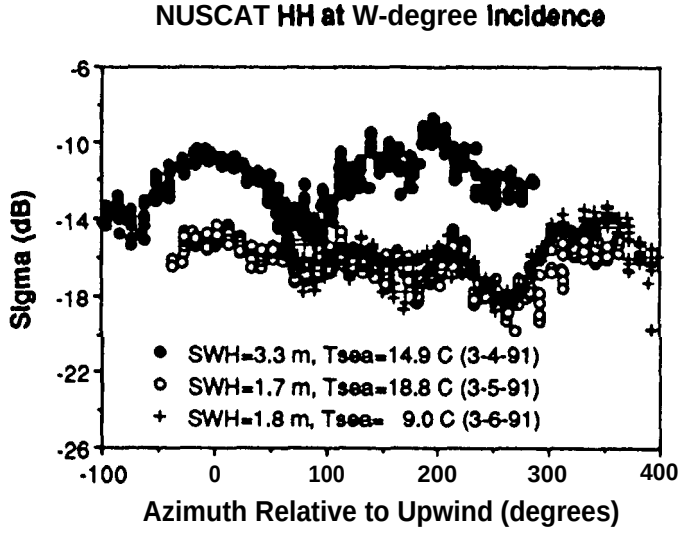
NUSCAT HH at W-degree Incidence
Sigma (dB)
-6
-10
-14
-18
-22
-26
-100
0
100
200
300
400
SWH=3.3 m, Tsea=14.9 C (3-4-91)
SWH=1.7 m, Tsea=18.8 C (3-5-91)
SWH=1.8 m, Tsea= 9.0 C (3-6-91)
Azimuth Relative to Upwind (degrees)

FIG 6

(a) NUSCAT HH Backscatter

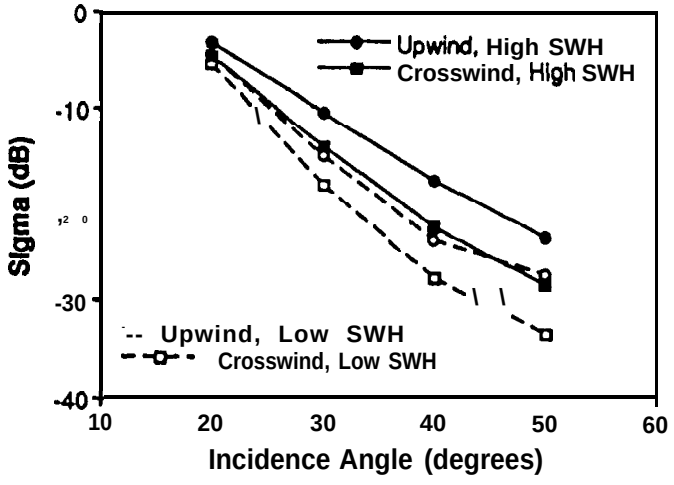

(b) C-SCAT W Backscatter

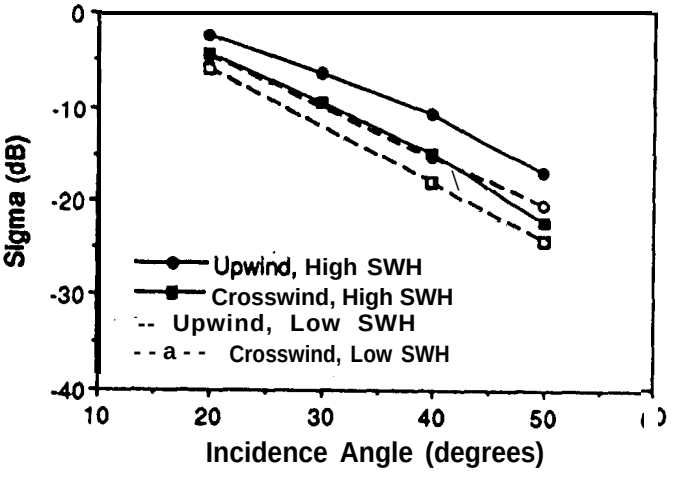

FIG 7

(a) Wind Speed Comparison

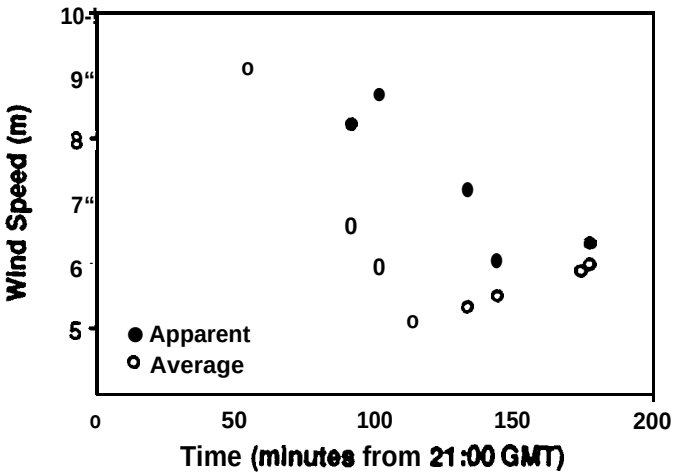

(b) Wind/VVave Direction Comparison

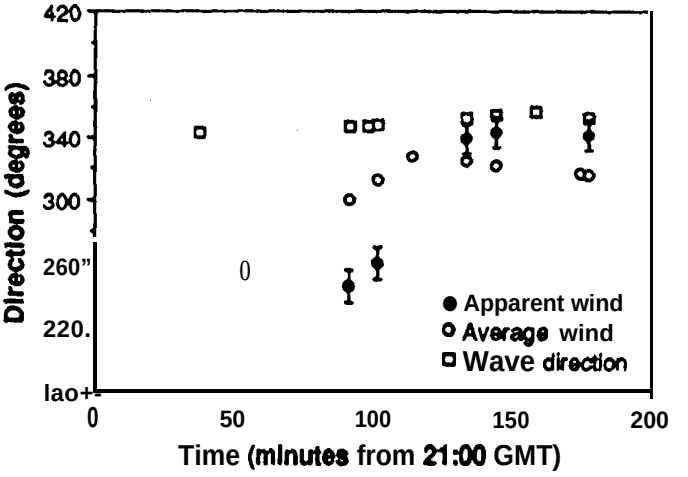

FIG 8

(8) NUSCAT W at W-degree incidence

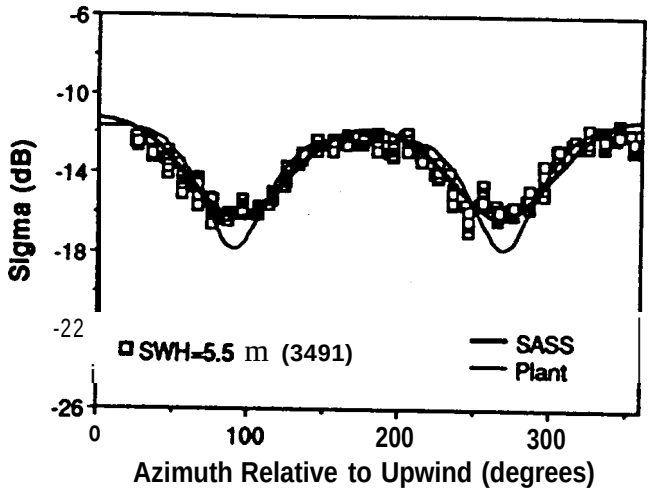

(b) C-SCAT W at 40-degree incidence

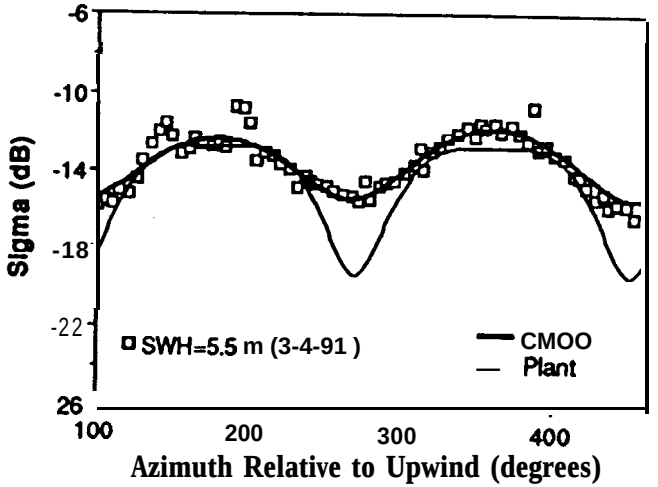

(c) NUSCAT HH at 40-degree Incidence

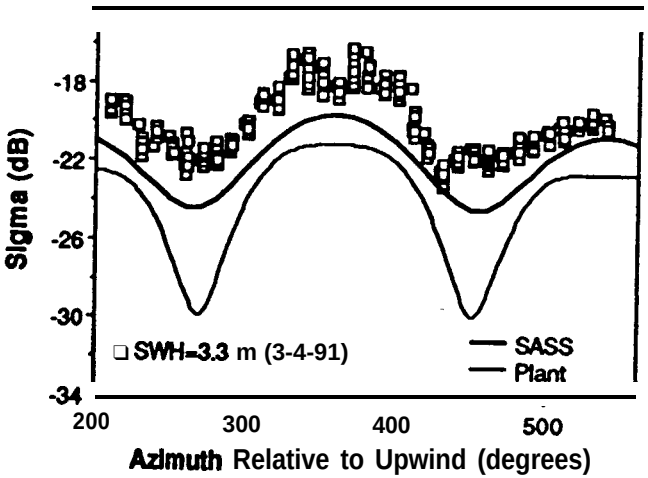

(d) C-SCAT W at 40-degree incidence

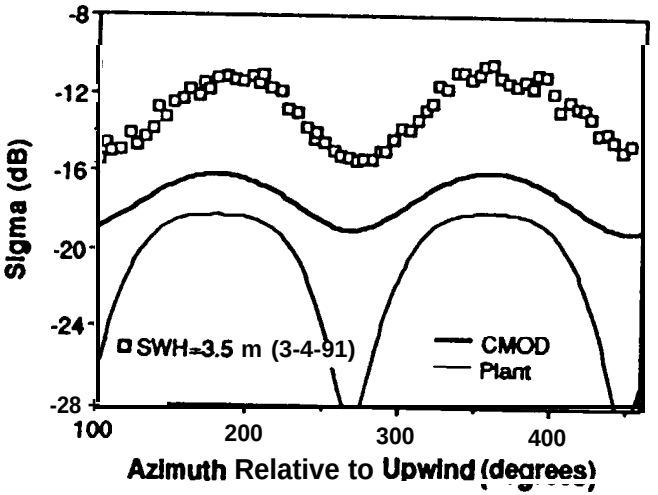

FIG 9

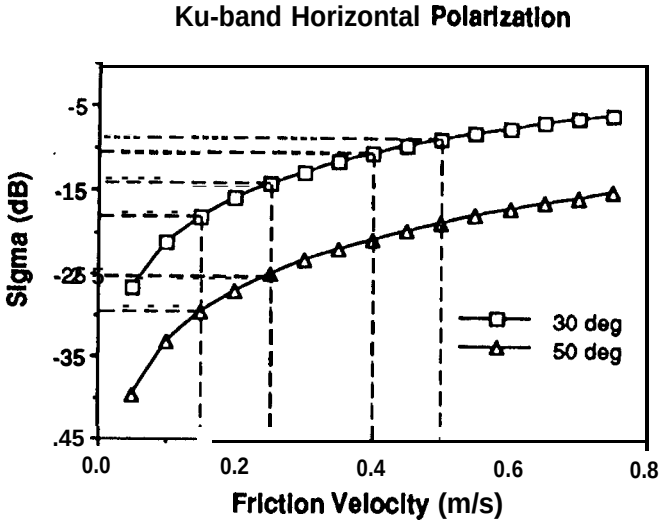
Ku-band Horizontal Polarization
Sigma (dB)
-5
-15
-25
-35
-45
0.0
0.2
0.4
0.6
0.8
Friction Velocity (m/s)
30 deg
50 deg

F(610

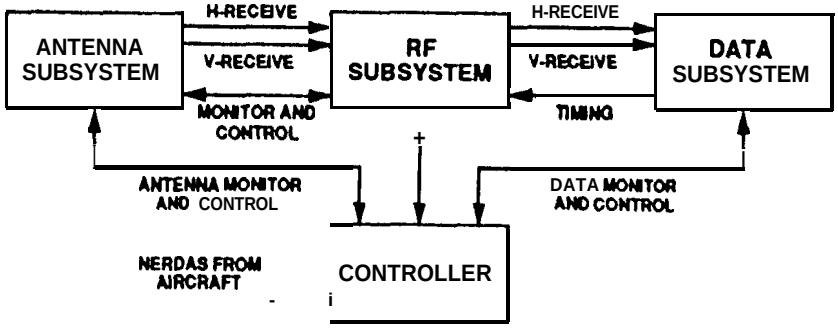

(a) NUSCAT SYSTEM BLOCK DIAGRAM

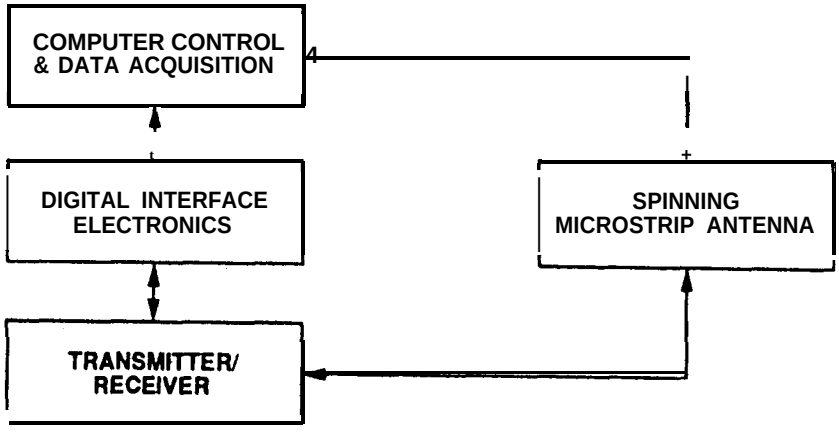

(b) C-SCAT SYSTEM BLOCK DIAGRAM

FIG, A1

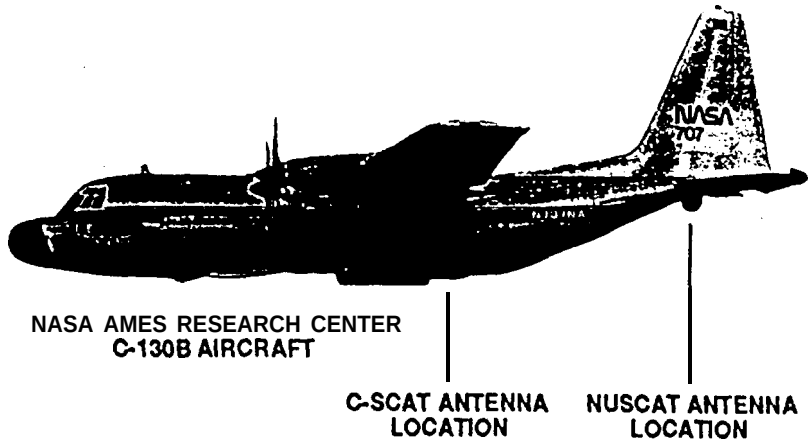
NASA
707
NASA AMES RESEARCH CENTER
C-130B AIRCRAFT
C-SCAT ANTENNA
LOCATION
NUSCAT ANTENNA
LOCATION

FIG A2

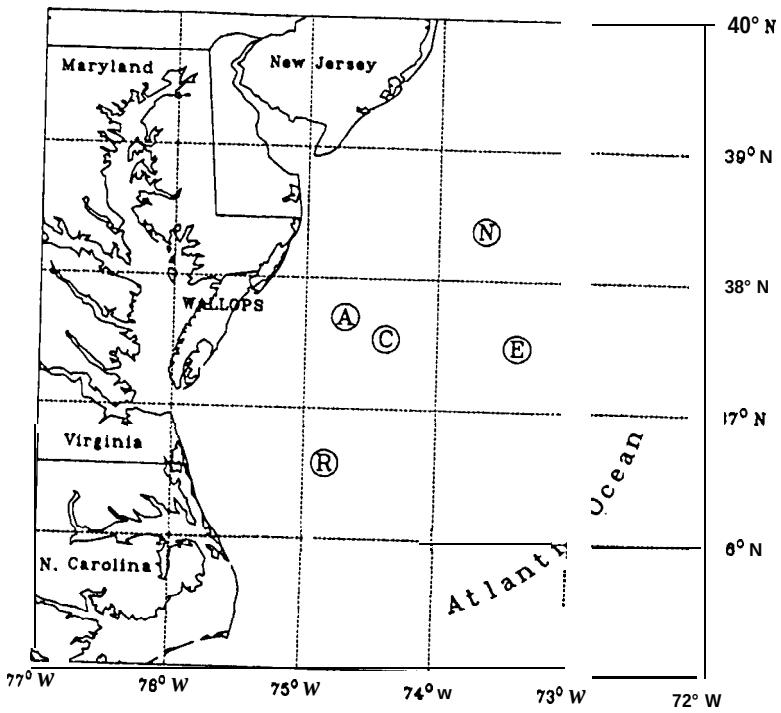
Maryland
New Jersey
WALLOPS
Virginia
N. Carolina
Atlantic Ocean
N
A
C
E
R
40° N
39° N
38° N
17° N
6° N
77° W
76° W
75° W
74° W
73° W
72° W

FIG A3

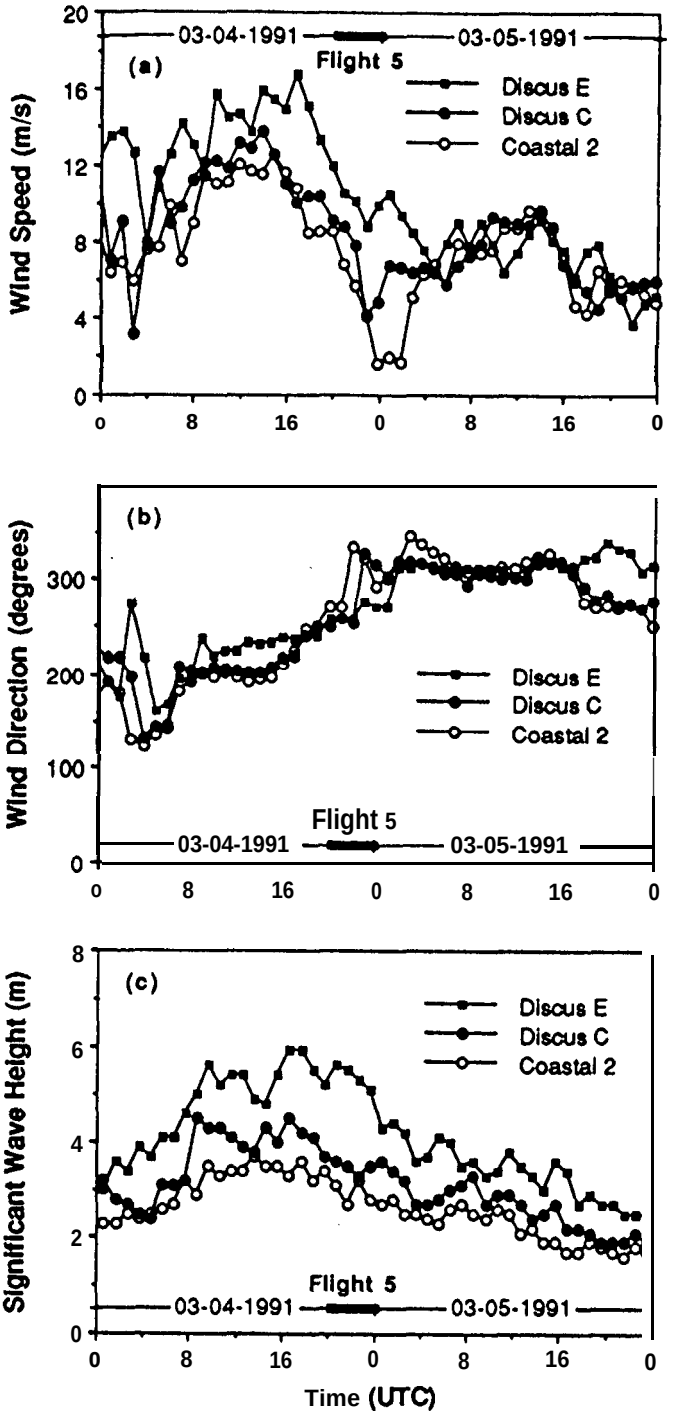
(a)
03-04-1991
03-05-1991
Flight 5
Discus E
Discus C
Coastal 2
Wind Speed (m/s)
(b)
Wind Direction (degrees)
(c)
Significant Wave Height (m)
Time (UTC)

FIG A4

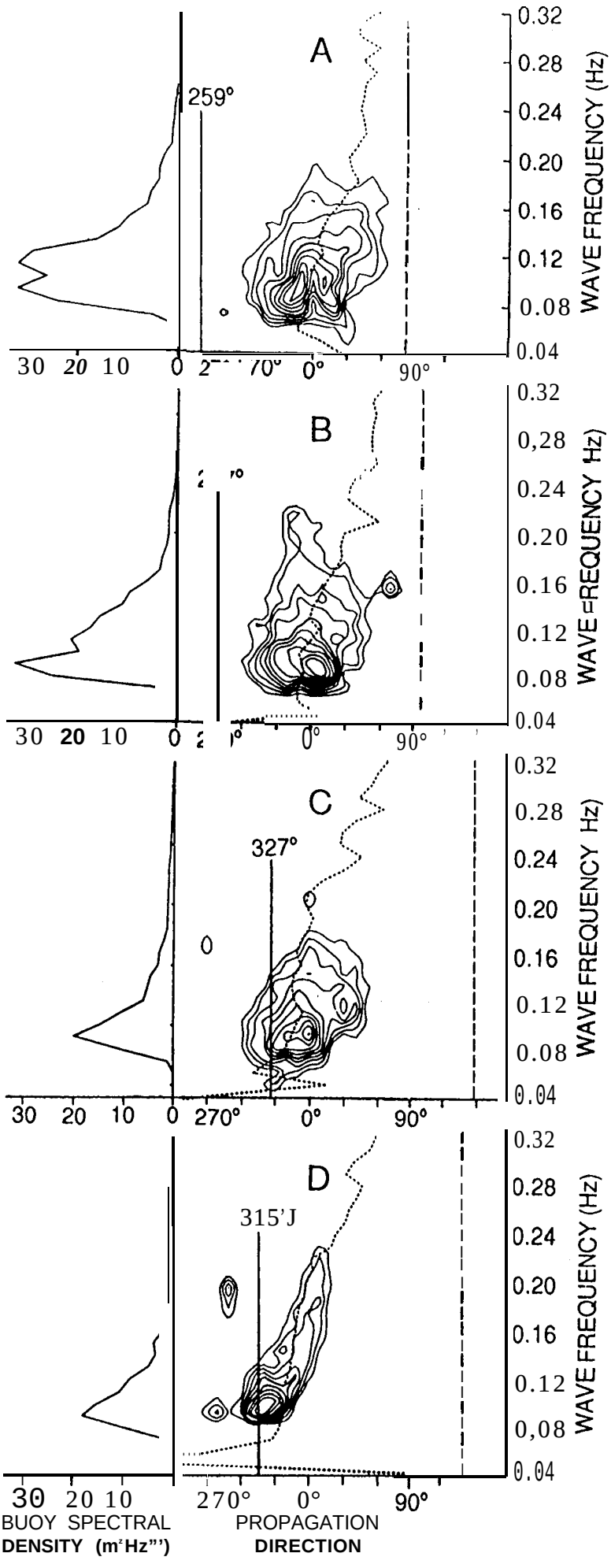
A
259°
B
C
327°
D
315'J
0.32
0.28
0.24
0.20
0.16
0.12
0.08
0.04
WAVE FREQUENCY (Hz)
30 20 10 0
270°
0°
90°
BUOY SPECTRAL DENSITY (m²Hz⁻¹)
PROPAGATION DIRECTION

FIG A5

DATE	Pol θ_0	U_N^A U_N^B $U_N^{\ell R}$	δU $\%E$	H_s	T_{air} T_{sea}
91-03-04	**VV 30**	**10.08 10.15 -na-**	**-na- -na-**	3.56	**12.1 14.9**
91-03-08	**VV 30**	1006811.16 9.67	-0.41 -4.07	1.58	5.88:7-
91-02-28	**VV 30**	11,5311,84 9.84	-0.24 -2.38	1.47	15,520.3
91-02-27	**VV 30**	11.2811.51 9.92	-0.16 -1.59	1.70	6,519.1
91-03-04	Vv 40	11.76 12.02 -na-	**-na- -na-**	5.49	**16.720.4**
91-03-08	Vv 40	12.6112.4112.22	**+0.46 +3.91**	1.72	**7.019,5**
91-02-28	Vv 40	12.0211.7712.27	**+0.51 +4.34**	1.45	**150520.3**
91-02-27	Vv 40	13.0312.8412.21	+0.45 +3.83	2.20	**7.220.6**
91-03-04	HH 20	**11.85 12.94 -na-**	**-na- -na-**	5.08	150720.4
91-03-08	HH 20	**10.9211.5812.28**	**+0.43** +3.63	1.90	6.719.6
91-03-08	HH 20	**11.5011.8112.63**	**+0.78 +6.58**	1.92	6.319.6
91-03-04	**HH 30**	9.6110.52 **-na-**	**-na- -na-**	5.27	**16.020.4**
91-03-06	**HH 30**	11.3711.4310.46	**+0.85 +8.84**	1.83	**6.919.6**
91-02-27	**HH 30**	11.1912.78 8.93	–0.68 –7.08	2,20	**7.220.6**
91-03-04	**HH 40**	10.9011.21 **-na-**	**-na- -na-**	**5.35**	**16.320.4**
91-03-08	**HH 40**	11.9911.7911.41	**+0.51** +4.68	**1,90**	**6.319.6**
91-02-27	**HH 40**	12.261300310.44	–0.46 –4.22	**2.20**	**7.420.6**
91-03-04	**HH** 60	**12.29 12.52 -na-**	**-na- -na-**	**5.10**	**15.720.4**
91-03-08	**HH 60**	12,8311.3813.97	+1.68 +13.7	1.81	6.919.6
91-03-08	**HH 60**	12.8011.6413.68	**+1.39 +11.3**	1.90	6.619.6

Table 1 Comparisons between high-wave (bold faced) and low-wave cases: Pol and θ_0 are antenna polarization and incidence angle in degrees. The apparent wind speed U_N^A is U_N^{hA} for high-wave cases (bold faced) or $U_N^{\ell A}$ for low-wave cases. Similarly, the buoy wind speed U_N^B *is* U_N^{hB} or $U_N^{\ell B}$ for high (bold faced) or low waves, respectively. $U_N^{\ell R}$ *is* the recovered wind speed. All wind speeds are in m $\cdot s^{-1}$ at 19.5 m. $\delta U = U_N^{\ell R} - U_N^{hA}$ and $\%E = 100(\delta U/U_N^{hA})$ are the difference in m $\cdot s^{-1}$ and the percent age error. H_s *is* significant wave height in m. T_{air} and T_{sea} *are* air and sea temperatures in "C.

FLT	DATE	Pol θ_0	*U(4)* (m/s)	H_s (m)	T_{air} (°C)	T_{sea} (°C)
5	91-03-04	HH 20	3.2	3.0	9.3	14.9
6	91-03-05	HH 20	4.4	1.8	10.2	18.8
5	91-03-04	HH 30	4.9	3.3	11.1	14.9
6	91-03-05	HH 30	4.3	1.7	10.2	18.8
7	91-03-06	HH 30	4 . 8	1.8	10.8	9.0
5	91-03-04	HH 40	5.5	3.3	11.3	14.9
6	91-03-05	HH 40	4.3	1.7	10.2	18.8
5	91-03-04	HH 50	4.4	3*4	10.6	14.9
7	91-03-06	HH 50	5.1	1.8	10.9	9.0

Table 2

FLT	DATE	Pol θ_0	U(4) (m/s)	H_s (m)	T_{air} (°C)	T_{sea} (°C)
5	91-03-04	VV 20	3.2	2.9	9.3	14.9
10	91-03-10	VV 20	4.5	1.0	5.9	16.0
5	91-03-04	VV 30	5.5	3.3	11.3	14.9
5	91-03-04	w 4 0	4.6	3.5	10.4	14.9
10	91-03-10	VV 40	4.5	1.0	5.8	16.0
5	91-03-04	w 5 0	5.0	3.3	11.1	14.9
10	91-03-10	VV 50	4.5	1.0	5.8	16.0

Table 3

RUN	DATE	TIME (UT)	LATITUDE (N) LONGITUDE (w)	T_{air} (“C) T_{sea} (“C)	H_s (m) ϕ_{wave} (°)	$U(12.9)$ (m · s^{-1}) ϕ_{wind} (°)	Exp. u_* (m) Cal. u_* (m)
24	91-03-05	21:09	36°50” 740 00”	11.0 18.8	2.5 324	3,33 310	0.16 0.13
25	91-03-05	23:09	37”00” 74°10”	11.5 19.5	1.9 315	3.72 284	0.26 0.14
27	91-03-06	17:17	37”17” 73”27”	16.0 19.6	2.1 315	6.95 175	0.37 0.25
29	91-03-07	20:32	43°00” 74°26’1	11,2 12.5	2.2 311	4.92 310	0,27 0.17

Table 4

RUN	DATE	TIME (UT)	LATITUDE(N)’ LONGITUDE (w)	T_{air} (“C) T_{sea} (“C)	H_s (m) ϕ_{wave} (^{0})	$U(12.9)$ (m .s^{-1}) ϕ_{wind} (°)	Exp. u_* (m) Cal. u_* (m)
16	91-03-04	18:56	3 6 ° 0 9 ” 75°15”	13.5 11,0	2.9 330	9.68 200	0.33 0.30
18	91-03-05	01:00	35”49” 75° 04”	12.1 14.5	2.7 330	9.67 253	0.40 0.33
19	91-03-05	02:00	35°49” 75°09”	11.9 14.0	2.6 342	8.61 277	0.37 0.30
20	91-03-05	03:08	35°49” 75°09”	11.8 14.0	2.2 324	8.78 288	0.41 0.30

Table 5

FLT	DATE	TIME (UT)	FLIGHT PATTERN	$\vec{U}(4)$ (m. s^{-1},°) CERC C E	H_s (m) CERC C E
1	91-02-27	**18:30-00:10**	Between A, C, and E	1.7-9.1 6.3-9.9 9.8-11.6 302-274 277-277 294-312	1.1-1.6 1.4-1.9 2,0-2.8
2	91-02-28	**21:00-00:40**	**Triangle** A, C, CERC then between A and C	3.4-6.1 8.4-12.6 9.6-12.1 **225-194** 21$218 229-228	0.9-1.0 1.1-1,6 1,3-1.8
3	91-03-01	**22:00-01:50**	Between A, C, and E	3.2-8.4 6.3-8.1 5.49.7 142-169 182-172 192-188	0.9-1.3 l. O-l.l 0.9-1.2
4	91-03-02	**21:00-00:50**	Between A, C, and E Some rain at altitude	6.0-11.7 6,2-8.8 8.8-13.0 233-195 271-194 270-209	2,9-3.2 3.0-3.3 3.6-4.1
5	91-03-04	**20:00-00:30**	**Triangle** C, N, and E Between A, C, and E	6.8-8.9 *4.2-9.2* 8.8-12.0 235-239 *327-251* 277-259	2.9-3.4 9.%9.7 4.3-5.6
6	91-03-05	**18:30-00:10**	Past N, in star pattern Between CERC-E, C-E	,??.5-7.1 4.5-6.0 3.7-7.8 9%?-913 281-279 329-325	1.7-2.0 1.9-2.2 2.5-2.9
7	11-03-06	**22:30-02:00**	Triangle C, N, and E then between C and E	7.48.810 .8-13.1 9,5-11.4 192-176 196-198 221-214	1.6-1.6 2.1-2.5 2.2-2.6
8	11-03-07	**20:30-02:20**	**5-leg** radiator A, C, E, N then between C and E	2.5-6.8 6.0-10.3 10.1-12.3 **318-341** 318-327 333-328	1.41.9 2.2-2.5 2.0-2.5
9	)1-03-08	**20:30-00:30**	**Triangle** C, N, and E then between C and E	8.$10.0 7.6-9.3 **9.9-11.0** 329-336 322-328 348-343	1.41.7 1.41.6 1.7-1.9
10	**1-03-09**	**20:30-02:40**	Between A, C, **and E**	**5.3-6.2 4.6-7.(I 6,4-7.6** **348-343 321-327 339-347**	**1.5-1.7 1.2-1.7 1.3-1.6**

Table Al Flight patterns and ocean conditions during S WADE. The events represented by bold-faced characters are used for the comparison of high and low waves at moderate wind speeds; the events represented by italic characters are for the comparison at light winds.